ENGINEERING TRANSACTIONS • *Engng. Trans.* • **47**, 1, 77–91, 1999
Polish Academy of Sciences • Institute of Fundamental Technological Research
10.24423/engtrans.615.1999

TORSION OF A SAINT-VENANT CYLINDER WITH A NON-SIMPLY CONNECTED CROSS-SECTION

T.F. JABŁOŃSKI

POLISH ACADEMY OF SCIENCES
INSTITUTE OF FUNDAMENTAL TECHNOLOGICAL RESEARCH
ul. Świętokrzyska 21, 00-049 Warsaw, Poland
e-mail: tjablon@ippt.gov.pl

and

U. ANDREAUS

UNIVERSITÀ DEGLI STUDI DI ROMA "LA SAPIENZA"
DIPARTIMENTO DI INGEGNERIA STRUTTURALE
& GEOTECNICA, FACOLTÀ DI INGEGNERIA
via Eudossiana 18, I-00184 Roma, Italy
e-mail: andreaus@scilla.ing.uniroma1.it

The Finite Element Method solution to the torsion problem of a linearly elastic, homogeneous, isotropic cylinder with a non-simply connected cross-section of variable wall thickness is presented. The computed displacement, warping, stress, strain and Mises invariant are shown for several shapes of the cross-section: a rectangle, a rectangle with a crossbar, and rings with sinusoidal boundaries of various amplitudes and periods. The computed results enable us to analyze the shape sensitivity to warping under torsion in thick-walled cylinders with complicated cross-sectional shapes.

1. INTRODUCTION

The classical problem of torsion of a prismatic bar (cylinder) possesses in general no analytical solution[1], even when formulated within the Saint Venant linearized theory. Among numerical methods, the finite element approach is prefe-

[1)] Except some regular simply connected cross-sections e.g. a circle, an ellipse, a square etc.

rable to the finite difference one because the boundary conditions are formulated in terms of displacement.

In everyday applications the walls of non-simply connected cylinders are usually thin enough to be sufficiently well approximated by shell elements. These are the elements many FEM packages are equipped with. In particular, they do not require much memory. Thus, a thin-walled solution can be obtained in a standard way using a typical workstation or even a strong PC.

The situation is quite different when the cylinder walls are not thin enough, or even worse – when they are of varying thickness. Then the shell elements are useless and full 3-D elements have to be employed. The drawbacks are: a huge memory (mainframe) requirement and a more complicated mesh defining phase. Alternatively, a combined analytic-numeric 2-D approach that takes advantage of the translational invariance of the cylinder and of the Saint Venant formulation should be worked out.

2. Formulation of the problem

Let us consider a linearly elastic, homogeneous, isotropic cylinder with a non-simply connected cross-section of variable wall thickness. The cylinder is schematically shown in Fig. 1. Its cross-section is defined by two curves Γ_i and Γ_o.

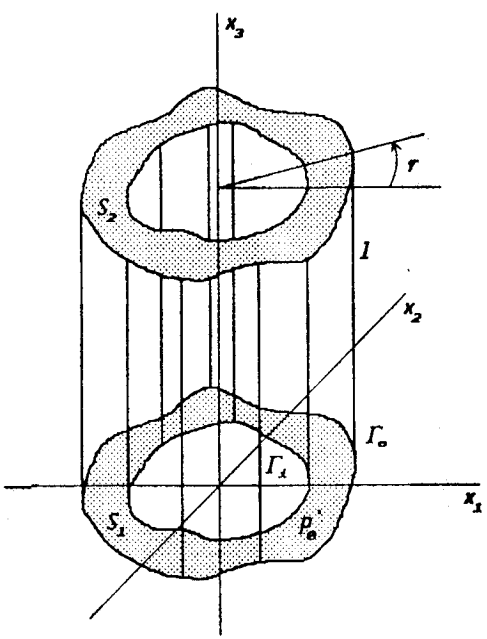

Fig. 1. The geometry and notation of the cylinder considered.

We assume that the end face S_1 is fixed in the x_1-x_2 plane, while the end face S_2 is rigidly rotated about the x_3-axis through an angle τ. The cylinder has length l and its every point is free to move in the x_3-direction except one point $p_0 \in S_1$, which is fixed. We also assume that there are no other forces on the lateral surface of the cylinder whereas the contact reaction forces will act on S_1 and S_2.

2.1. 2-D formulation

The Saint Venant torsion problem can be reduced in a classical way [1] to a 2-D Dirichlet (Neumann) problem for Poisson (Laplace) equation with the unknown Prandtl stress flow (Saint Venant warping) function. The difficulty of solving this problem for non-simply connected domains lies not only in the complexity of their shapes. More critical is the fact that the solution values on the boundary curves Γ_j, $j = 1, 2, \ldots$ are not known *a priori*, but only indirectly through an integral relation involving the gradient of the solution, the torsion angle and some material and geometric constants. The above observation suggests that an iterative approach could be successful in that case.

For the sake of completeness, here we briefly present the iterative scheme the author[2] has developed together with FRANCESCO dELL'ISOLA from Università di Roma "La Sapienza". This scheme is further discussed in [2]. For simplicity we restrict ourselves here to a one-hole-domain Ω with inner boundary Γ_i and outer boundary Γ_o.

Let α be a given real constant. Then for every $\gamma \in \mathbb{R}$, let u_γ be the solution to the following Dirichlet problem:

$$\begin{cases} \Delta u_\gamma = -2, \\ u_\gamma|_{\Gamma_i} = \gamma, \quad u_\gamma|_{\Gamma_0} = 0. \end{cases} \tag{2.1}$$

The u_γ from (2.1) will be the Prandtl stress flow solution if and only if we pick up γ such that

$$\int_{\Gamma_i} \nabla u_\gamma \cdot \mathbf{n} = \alpha \tag{2.2}$$

where $\mathbf{n}$ is the unit outer normal. Thus, solution of the torsion problem is reduced to finding zero of the following real function f:

$$\mathbb{R} \ni \gamma \xrightarrow{f} (\alpha - \int_{\Gamma_i} \nabla u_\gamma \cdot \mathbf{n}) \in \mathbb{R}. \tag{2.3}$$

[2] In fact, $\alpha = -2A_{\Gamma_i}$, where A_{Γ_i} is the area of the domain bounded by Γ_i.

Let us notice that each evaluation of f requires solving a Poisson equation for a non-simply connected 2-D domain, which can be numerically expensive.

However, making use of the maximum principle for subharmonic functions, it can be proven that f *is a monotonic, linear function of* γ. This fact can be deduced also from physical arguments after recalling the well known analogies based on the equivalence of the (Poisson) torsion equation to the membrane displacement equation or to the capacitor electrostatic potential equation.

Since f is linear, it suffices to solve (2.1) only twice in order to find the right pair (γ, u_γ) for a given α. This is true for a one-hole-domain. In a general n-hole case we arrive at the set of n linear equations for the unknown $\gamma_1, \gamma_2, \ldots, \gamma_n$ Prandtl function values on the boundaries of the n holes.

The attractiveness of the technique presented here consists in reducing the problem to two dimensions, which saves a lot of computer memory, as compared to a straightforward 3-D approach. The bottleneck of the method is that we have to solve numerically Poisson equation for each evaluation of the function f. Thus, in order to make the method effective, a fast and effortless numerical procedure should be worked out and carefully adjusted for each given class of the cylinder cross-sections. Theory and experience show that in the case of Poisson equation, a variant of the finite difference method should be most suitable. Also the finite element method could be used to solve (2.1), provided suitable elements, e.g., membrane elements were at our disposal. In any case, elaborating such a procedure is a substantial numerical task and the results of its implementation will be presented elsewere.

2.2. 3-D formulation

In a straightforward 3-D formulation we build up the FEM solution from 8-nodal 3-D linearly elastic elements. Because of employing Gaussian interpolation it suffices to take only two layers along the wall thickness. Nevertheless, the total number of the elements used is quite large since 1) the meshed cylinder should be high enough for the end faces perturbations to become negligible, 2) the shape of each element should be kept not too different from a cube.

The boundary conditions in our torsion problem can be written in terms of the displacement vector function $\mathbf{u}(x_1, x_2, x_3) = [u_1, u_2, u_3]$ as follows:

$$
\begin{array}{lll}
 & \text{on } S_1\text{:} & \text{on } S_2\text{:} \\
 & u_1(x_1, x_2, 0) = 0, & u_1(x_1, x_2, l) = -\tau x_2, \\
(2.4) & u_2(x_1, x_2, 0) = 0, & u_2(x_1, x_2, l) = \tau x_1, \\
 & u_3(p_0) = 0, &
\end{array}
$$

in order that the Saint-Venant's solution [3] holds along the whole cylinder. The conditions in the above form can be directly applied to the appropriate nodes of the mesh, provided that the nodal coordinates x_1, x_2 are explicitly known.

Within the *ABAQUS* package that we used for our 3-D computation it was impossible to refer *a priori* to the coordinates of the constructed nodes neither by the *ABAQUS* internal language for preparing job-input files, nor by the supplied external preprocessor, nor even using allowable low level external FORTRAN procedures[3].

3. Generation of the mesh

Taking into account that the *ABAQUS* language for preparing job-input files appeared to be quite primitive and oldfashioned; also in many other aspects, we decided to employ *Mathematica* computer system to prepare the complete job-input files for *ABAQUS* from the scratch. The advantage is that by writing a short and simple *Mathematica* package we automated the tedious process of defining mesh and displacement boundary conditions for complicated, but easily modifiable geometries. The package is written in such a way that the crucial geometrical and material parameters of the structure under torsion are the package input variables. To illustrate our idea we present below the fragment of the *Mathematica* procedure that generates the *ABAQUS* job-input files for cylindrical rings with sinusoidal boundaries of various amplitudes and periods.

```
(* 12 hunch ring with the ripple factor:  0.5 *)
t1205 := meshtor[ 10, 0.5, 12, 12, 20, 0.100, 0.05, 0.06 ]
  ..............
  ..............
meshtor::usage = "meshtor[ tau, ripple, n, m, nsli, h, rin, rout ], where:
tau - torsion angle [deg],
ripple - the hunch depth factor (should be:  0 <= ripple < 1),
n - number of hunches,
m - number of nodes per 1 hunch,
nsli - number of slices,
h - total height [m],
rin - inner radius [m],
rout - outer radius [m]
";
meshtor[ tau_, ripple_, n_, m_, nsli_, h_, rin_, rout_ ] := Module[
 { amp,tors,step,j,jnod,g1,g2,g3,rob
  ,inner={},outer={},middle={}
 },
  amp = ripple*(rout-rin);
  step = 2 Pi n m;
  tors = Pi tau  180;
```

[3] Because the nodal coordinate variables were not included in the appropriate EXTERNAL declarations of the user supplied procedures.

```
fi = 0;
While[ N[ fi ] <= N[ 2 Pi ],
  AppendTo[ inner, { rin*Cos[fi], rin*Sin[fi] } ];
  rob = rout + amp*Cos[ n*fi ];
  AppendTo[ outer, { rob*Cos[fi], rob*Sin[fi] } ];
  rob = (rin + rob)  2;
  AppendTo[ middle, { rob*Cos[fi], rob*Sin[fi] } ];
  fi += step;
];

jnod = Length[inner];
g1 = ListPlot[ inner, AspectRatio->Automatic, DisplayFunction->Identity];
g2 = ListPlot[ middle, AspectRatio->Automatic, DisplayFunction->Identity];
g3 = ListPlot[ outer, AspectRatio->Automatic, DisplayFunction->Identity];
g =  Show[ {g1,g2,g3}, DisplayFunction -> $DisplayFunction];

Print["*HEADING"];
Print["  BIKE_TORPEDO____",n,"_HUNCHES____RIPPLE_FACTOR_",ripple];
Print["**                              "];
Print["**  output directives           "];
Print["**                              "];
Print["*RESTART, WRITE, FREQUENCY=1 "];
Print["**                              "];
Print["**                              "];
Print["**  generation of nodes         "];
Print["**                              "];
Print["** bottom outer boundary        "];
Print["**                              "];
Print["*NODE,  NSET=N_BOUTER           "];
Do[
  Print["  ",11000+j,", ",outer[[j,1]]  N,", ",outer[[j,2]]  N,",  0" ];
,{j,1,jnod} ];
.................
.................
.................
```

Thus, using *Mathematica* we can readily produce complete *ABAQUS* job--input files for "smoothly" modified geometry and therefore effectively, investigate the shape sensitivity of a structure under torsion.

4. Numerical results

We performed computations for the following three types of the cylinder cross--section: a rectangle, the same rectangle but with a crossbar (two-hole-domain), and rings with sinusoidal boundaries of various amplitudes and periods. All the results are presented in tabulated and in graphical form according to the same scheme described below.

For each case, the *ABAQUS* job-input file was prepared using *Mathematica*. The node coordinates with the *ABAQUS* computed values of the displacement,

strain, stress and von Mises invariant were tabulated and the related Post Script graphic was generated. The graphical representation of the results includes:

- a general 3-D view of the cylinder displacement under torsion,
- the 3-D contour map of the von Mises invariant values over the whole cylinder,
- the detailed 3-D plots of the middle slice of the cylinder (the central layer of the elements) presenting: the warping of the middle slice, the torsion of the slice, the 2-D contour maps of the two dominant[4] stress tensor components σ_{13}, σ_{23} and the contour maps of the dominant strain tensor component ϵ_{13} and of the von Mises invariant

$$q = \sqrt{\frac{3}{2} \sum_{i,j=1}^{3} \sigma_{ij}\sigma_{ij}}$$

over the slice cross-section.

In all cases the cylinders are made of steel with Young's modulus $2.1 \cdot 10^8$ kg/mm^2 and Poisson's ratio 0.3, and the torsion angle is $\tau = 10\,\mathrm{deg}$.

The numerical examples presented below serve merely as the canonical ones with respect to real industrial applications. They are useful for validating our 3-D formulation of the torsion problem and for testing the performance and accuracy of our numerical implementation, as well as its applicability to industrial problems.

4.1. The rectangle

The dimensions of the cylinder are $15 \times 10 \times 12.5\,\mathrm{cm}$ ($x_1 \times x_2 \times x_3$) and the wall thickness is 0.5 cm. The numbers of elements taken are $2 \cdot (45 \times 30 \times 25)$, respectively. The 3-D view of the cylinder displacement under torsion and the 3-D contour map of the von Mises invariant are shown in Figs. 2 a, b, respectively. The warping and the torsion of the middle slice of the cylinder are presented in Fig. 5 a.

4.2. The rectangle with a crossbar

The cylinder has the same dimensions and the wall thickness as described in Subsec. 4.1. However, an extra crossbar is added. It is placed along the x_2-coordinate at 1/3 of the x_1-length of the cylinder. The 3-D views for that case are presented in Fig. 3, while the warping and the torsion of the central layer are shown in Fig. 5 b.

[4] Theoretically, these are the only nonzero components; the dominance is of order of the *ABAQUS* accuracy of computations – we can see that six digits are significant.

The influence of the crossbar can be estimated from comparing the respective figures. The differences in warping are worth noticing, as well as the changes in the distribution of the von Mises invariant q values over the cylinder walls. The range of q is $4.72 \cdot 10^6 - 1.94 \cdot 10^7$ for the empty cylinder and $1.56 \cdot 10^5 - 2.12 \cdot 10^7$ for the cylinder with the crossbar. The green color in Fig. 2 b corresponds to $q = 1.15 \cdot 10^7$. On the other hand, in the Fig. 3 b, the green color corresponds to $q = 9.9 \cdot 10^6$ and the yellow to $q = 1.4 \cdot 10^7$.

As we can see, the redistribution of equivalent stress over more complicated non-simply connected structures obtained by introducing crossbars, can be successfully analyzed within our formulation of the torsion problem.

4.3. The ring with varying thickness

We have analyzed the shape sensitivity to warping of ringed cylinders by changing the period and the amplitude of a sinusoidal outer boundary of the cylinder cross-section. Starting from a perfectly round ring with the inner radius 5 cm and with the constant thickness equal to 1 cm, we have changed the number of humps on the outer wall from 1 to 48 and the height of the humps[5] in the range 0 – 9 mm. The number of elements taken are $2 \cdot (20 \times 120 \div 192)$.

In Fig. 4 and Fig. 5 c we show the results for the cylinder with 3 humps and the ripple factor equal to 0.5. It is worth noticing that in the right plot of Fig. 5 c, the inner radius of the cylinder increases under torsion. This is a simple consequence of the volume conservation law and it confirms the validity of the computations performed.

As one could expect, the Mises invariant q attains its maximum at the thinnest parts of the cylinder wall, while the minimum of q is reached at the thickest parts. In Fig. 6 we show the computed maximal and minimal values of the Mises invariant versus the ripple factor for the cylinder with fixed number of humps = 12. In Fig. 7 the ripple factor is fixed and equals 0.5 and the extremal q-values are ploted versus the number of humps. Again, the computed curves look reasonably and validate our numerical formulation. For example, the maximum of q increases[6] for larger ripple factor, since the minimal wall thickness decreases. Similarly, it is naturally expected that extremal q-values are almost constant for a fixed ripple factor and they change substantially only when a hump (or humps) of fixed height just arrives on the lateral surface of a homogeneous round cylinder[7].

---

[5] The maximal thickness of the cylinder wall is kept constant; we define the *ripple factor* as the ratio of the hump height to the wall thickness, so it is within $0.0 \div 0.9$ in our case.

[6] Up to infinity as ripple factor tends to 1.

[7] When the number of humps is around 50, the cylinder becomes a sort of toothed wheel.

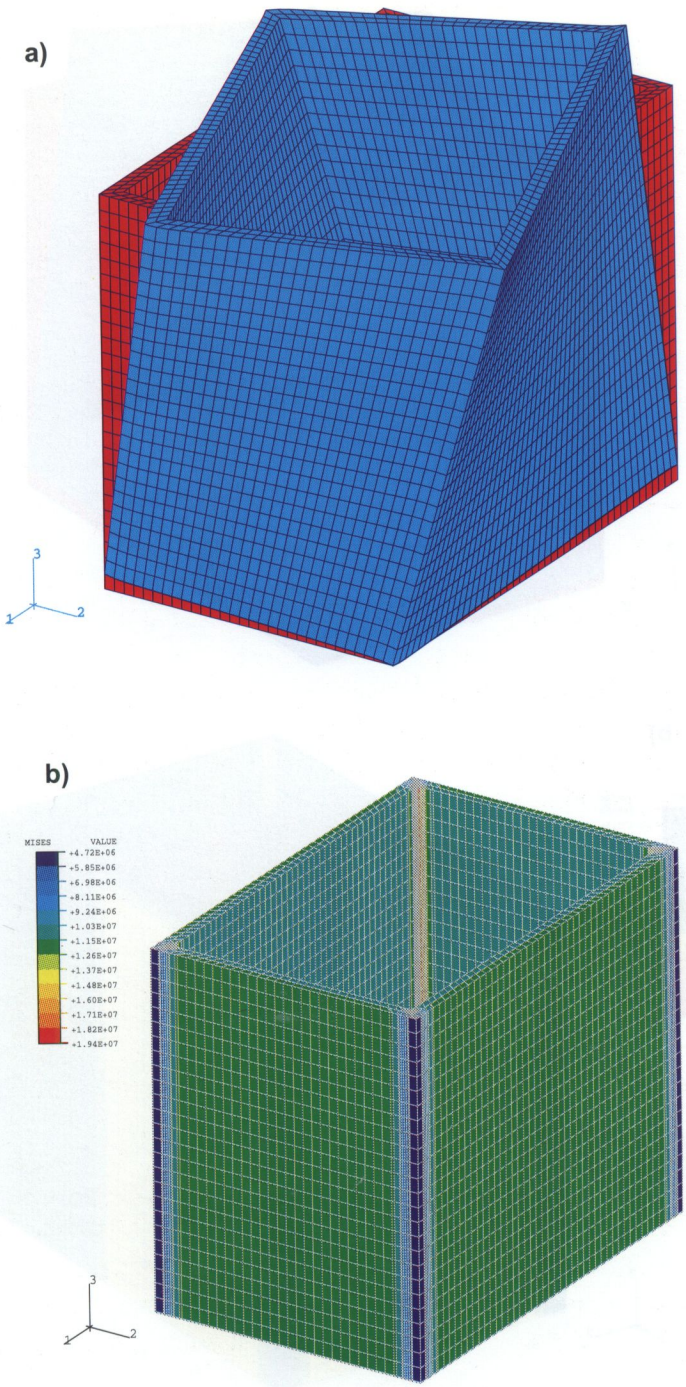

FIG. 2. Cross-section: the rectangle; a) displacement under torsion and b) the 3-D contour map of the Mises invariant.

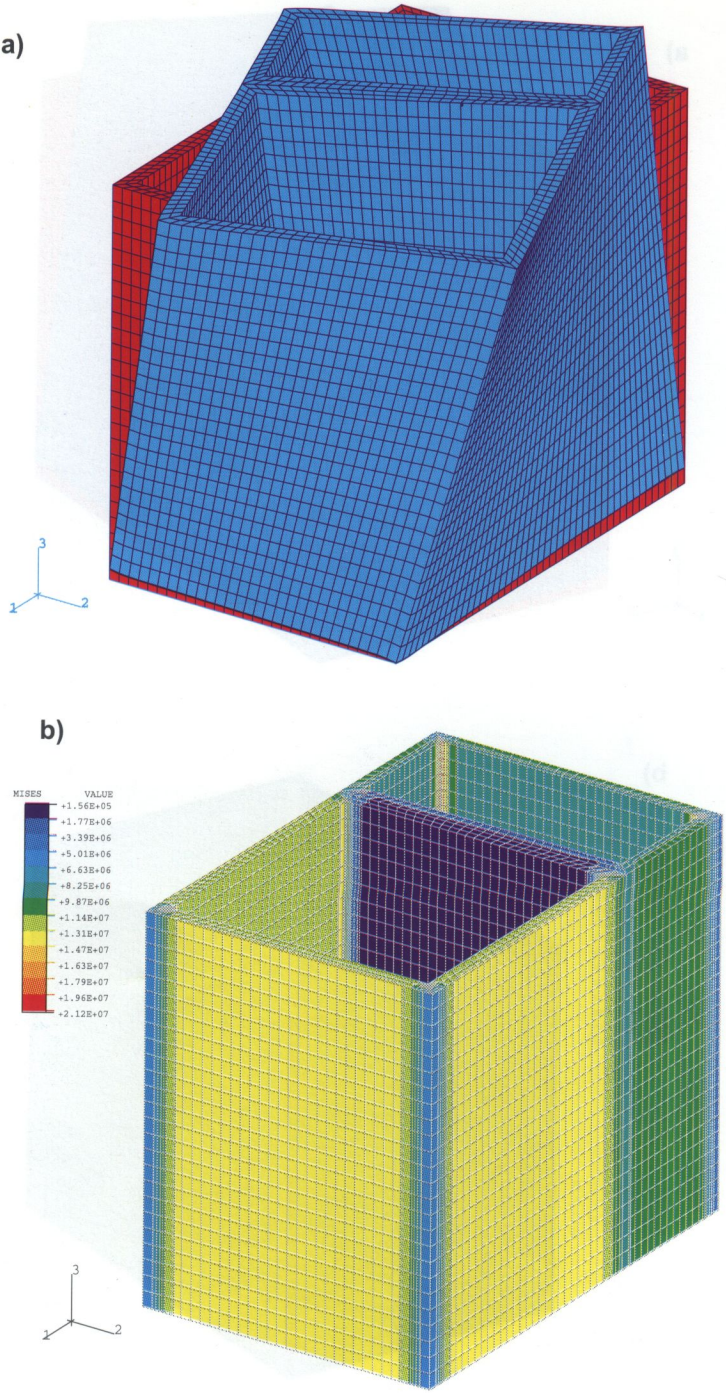

FIG. 3. Cross-section: the rectangle with a crossbar; a) displacement under torsion and b) the 3-D contour map of the Mises invariant.

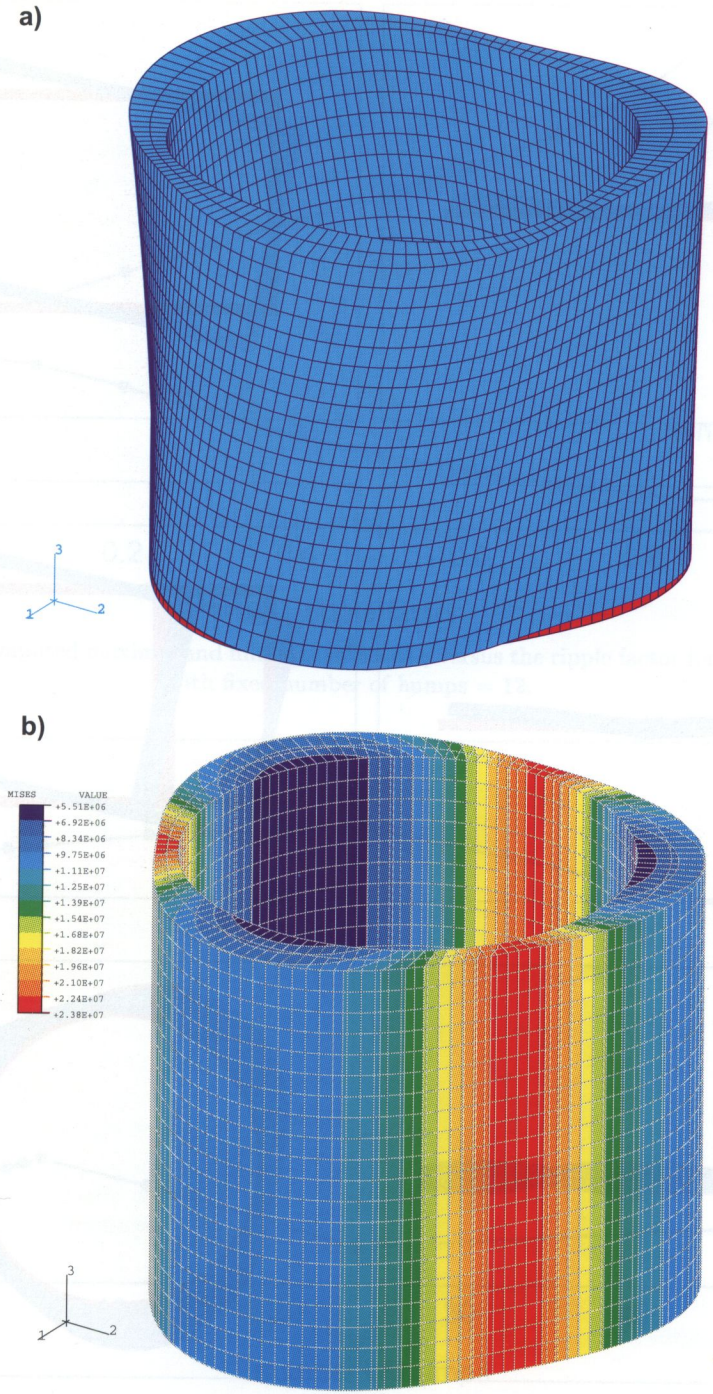

FIG. 4. Cross-section: the ring with varying thickness (3 humps, ripple factor = 0.5); a) displacement under torsion and b) the 3-D contour map of the Mises invariant.

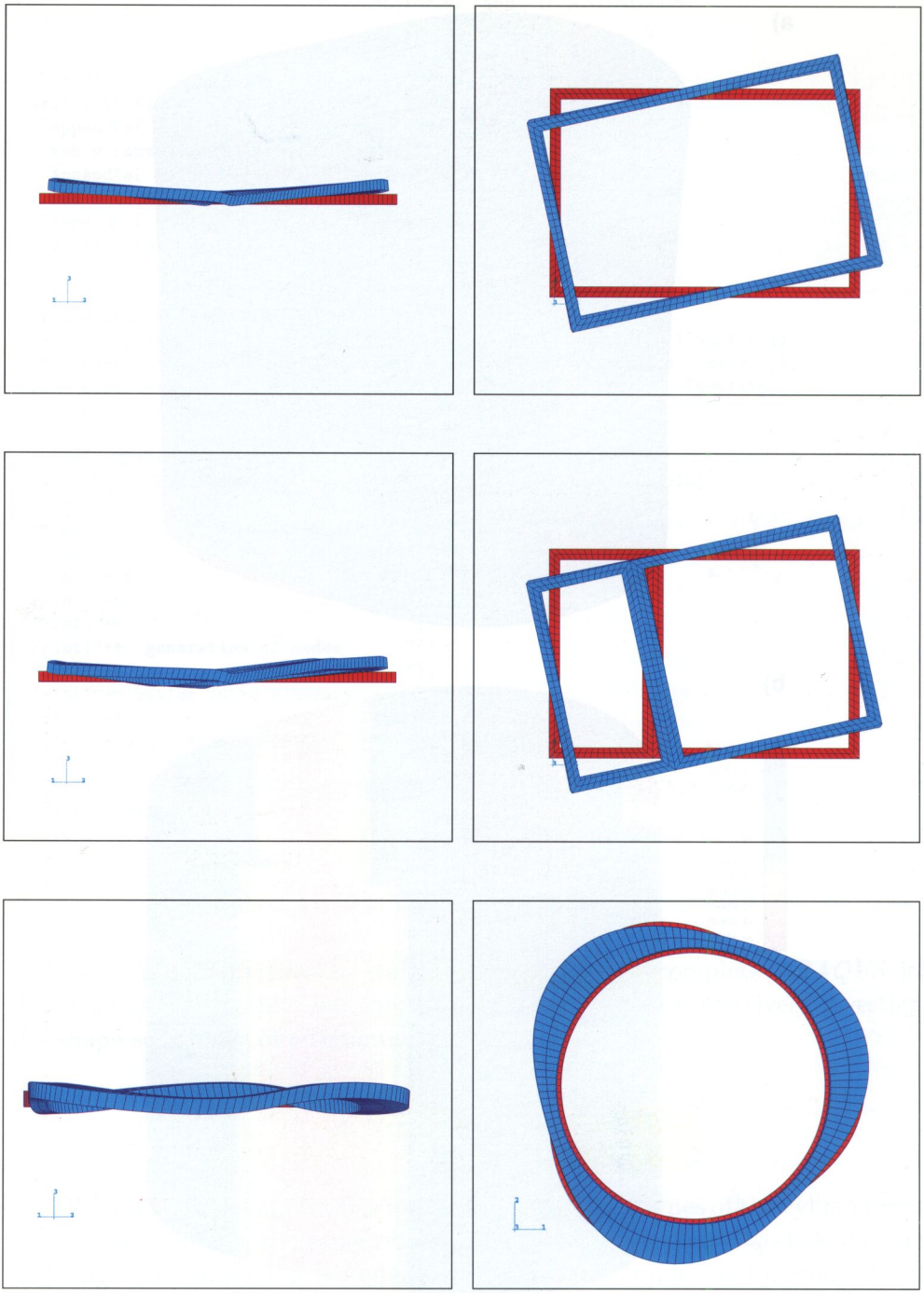

FIG. 5. Warping and torsion of the cylinder central layer with the cross-section: a) the rectangle, b) the rectangle with a crossbar, c) the ring with varying thickness (3 humps, ripple factor = 0.5).

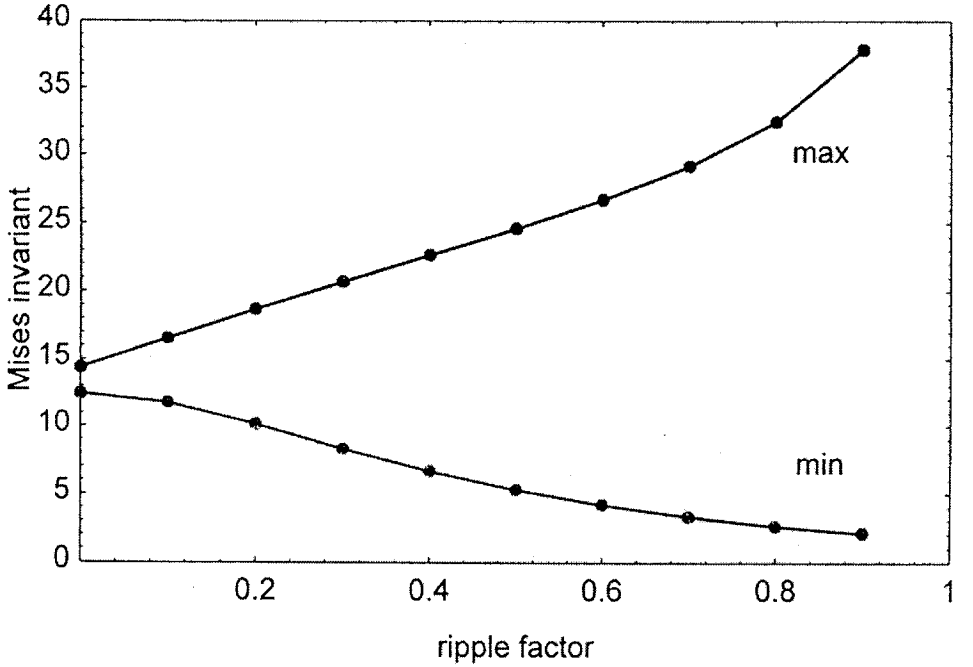

FIG. 6. The computed maximal and minimal values of q versus the ripple factor for the cylinder with fixed number of humps = 12.

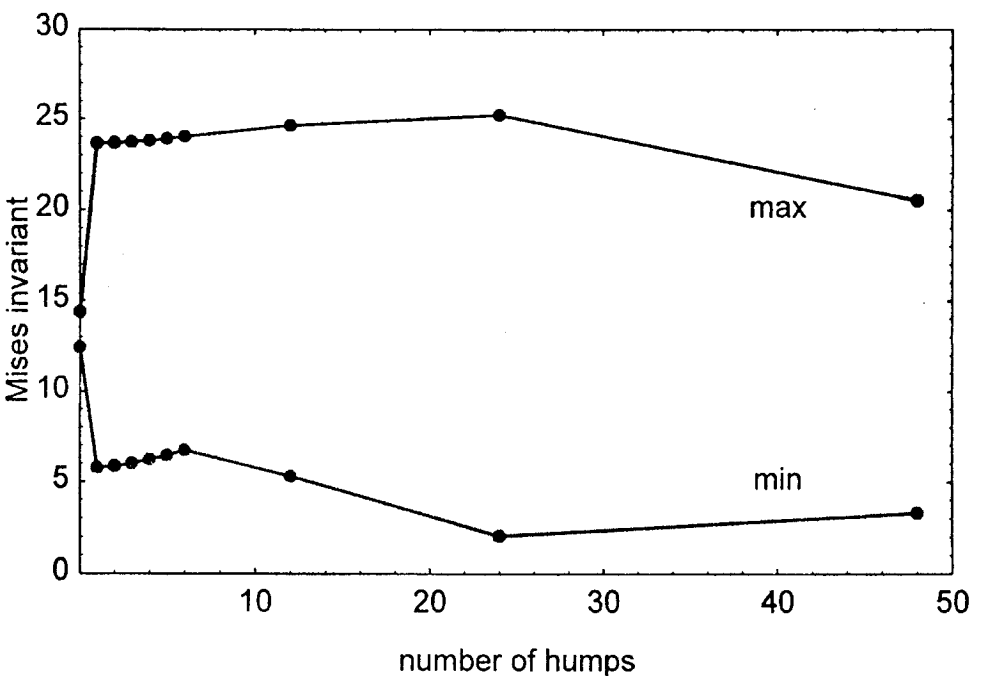

FIG. 7. The computed maximal and minimal values of q versus the number of humps for the cylinder with fixed ripple factor = 0.5.

4.4. Validation of the results

Our numerical formulation can be further validated by comparing our computation to the case when the analytical solution is known. Fortunately, there exists one for a cylinder with a finite, but not small, wall thickness. Let us consider the hollow circular shaft of inner radius a and outer radius b, twisted by the angle β per unit length of the bar. It is easy to guess the Prandtl torsion function u in this case:

$$u = c\,(x_1^2 + x_2^2 - b^2). \tag{4.1}$$

With the constant $c = -\frac{1}{2}\beta G$, G being Lamé's coefficient, the function u from (4.1) satisfies the Poisson equation $\Delta u = -2GB$ in the cross-section of the bar and the conditions $u|_{\Gamma_0} = 0$, $u|_{\Gamma_1} = \frac{1}{2}\beta G(b^2 - a^2)$ on its boundaries Γ_0 and Γ_1. Consequently, using u, we can express (cf. [1]) the nonvanishing stress components σ_{13}, σ_{23} as:

$$\sigma_{13} = \frac{\partial u}{\partial x_2} = -\beta G x_2, \qquad \sigma_{23} = -\frac{\partial u}{\partial x_1} = \beta G x_1. \tag{4.2}$$

Furthermore, we can relate the warping function w to the Prandtl function u by the equations

$$\frac{\partial w}{\partial x_1} = \frac{1}{\beta G}\frac{\partial u}{\partial x_2} + x_2, \qquad \frac{\partial w}{\partial x_2} = -\frac{1}{\beta G}\frac{\partial u}{\partial x_1} - x_1. \tag{4.3}$$

From (4.2) and (4.3) we see that $w \equiv 0$ and there is no warping in this case.

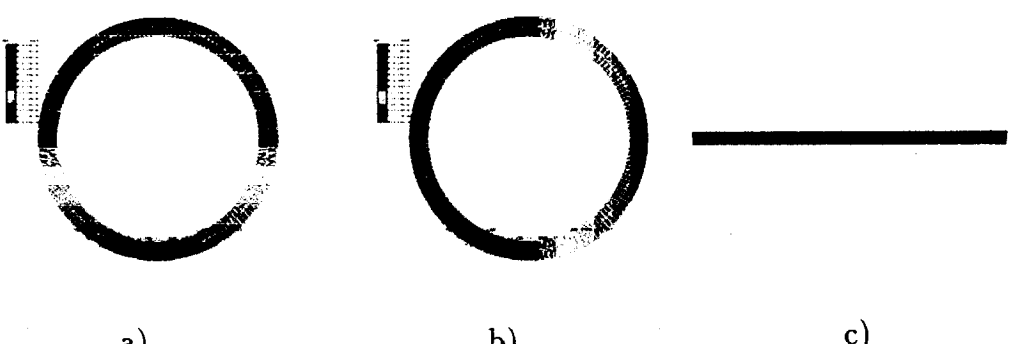

FIG. 8. Cross-section: the ring of constant thickness; a) σ_{13} stress component, a) σ_{23} stress component, c) null warping.

Our numerical results for the hollow circular shaft are in perfect agreement with the above analytical conclusions: we obtained purely (within six digits accuracy) x_2 dependence of the σ_{13} stress component, entirely x_1 dependence of σ_{23} and no warping in the x_3 direction. These facts are shown in Fig. 8 a, b, c, respectively.

5. Conclusion

The shape sensitivity to warping under torsion in thick-walled cylinders with complicated, multi-connected cross-sections can be effectively investigated for industrial applications using the proposed 3D-FEM approach with the essential help of the *Mathematica* computer system for automated preparation from the scratch the complete FEM job-input files.

Acknowledgments

The authors express their gratitude to E. Postek for his valuable help in employing *ABAQUS* package for the FEM computation. They also wish to thank F. dell'Isola for his encouragement, support and useful discussions.

References

1. A.P. Boresi, P.P. Lynn, *Elasticity in engineering mechanics*, Prentice-Hall, Inc. Englewood Cliffs, New Jersey 1974.
2. F. dell'Isola, G.C. Ruta, *Outlooks in Saint-Venant theory III; Torsion and Flexure in sections of variable thickness by formal expansions*, Arch. Mech., **49**, 2, pp. 321–343, 1997.
3. A.J.C. Barré de Saint-Venant, *Mémoire sur la torsion des prismes*, Mémoires par Divers Savants de l'Academie des Sciences (Paris), **14**, 233, 1859.

Received new version June 26, 1998.